PHYSICAL REVIEW D VOLUME 23, NUMBER 1 1 JANUARY 1981

Electromagnetic production of trimuons in muon scattering: Bethe-Heitler reactions with muon and heavy-lepton pairs

V. Ganapathi and J. Smith
Institute for Theoretical Physics, State University of New York, Stony Brook, New York 11794
(Received 12 June 1980)

We analyze the Bethe-Heitler production of muon and heavy-lepton pairs using high-energy muon beams on a variety of targets. We give results for coherent production from a nucleus, for incoherent production from individual protons and neutrons, and for deep-inelastic production. Differential distributions are presented for the final leptons and the effects of experimental cuts are considered. This work complements our previous study of trimuon production via muon radiation, Compton radiation, and hadronic final-state interactions.

I. INTRODUCTION

The production of lepton pairs in muon-initiated reactions, which is normally referred to as trident production, has been investigated by a variety of authors. Brodsky and Ting[1] first calculated some triple-differential cross sections. About the same time Bjorken and Chen[2] and independently Henry[3] wrote down analytical expressions for the trident cross sections as sevenfold integrals. No attempt was made to numerically evaluate the cross section until the paper of Tannenbaum[4] who computed the cross section for 12-GeV muon beams, including correctly the effects of Fermi statistics for the muons. Subsequently Homma *et al.*[5] gave some long trace formulas for the differential cross section, without attempting any numerical results. Recently we calculated the exact cross sections for the charge-conjugation-odd Compton radiation of muon pairs and the hadronic radiation of muon pairs in muon-initiated reactions and presented results for a range of beam energies.[6] Independently, Barger *et al.*[7] did similar calculations for a wide variety of production processes at a muon beam energy of 280 GeV. So far there has not been any detailed discussion of heavy-lepton contributions to trimuon production and we would like to cover this subject in this paper. We therefore present results of an investigation of the even-charge-conjugation Bethe-Heitler-type reactions and give cross sections and distributions for the production of muon pairs, τ pairs ($m_\tau = 1.78\ \mathrm{GeV}/c^2$), and, for interpolation purposes, a hypothetical lepton pair $L^\pm$ with mass $m_L = 4.8\ \mathrm{GeV}/c^2$. The production of heavy leptons via weak interactions has been discussed by Albright and Shrock.[8]

The results which are available in the literature on Bethe-Heitler reactions deal primarily with final-state muons. Experiments have been performed at low muon energies[9,10] and at high energies[11] to check the basic cross sections. We would like to present results for cross sections and distributions when heavy leptons are produced and compare them with results on direct muon production. This is relevant because several high-energy experiments are under way to study multimuon production in muon beams. We have in mind the Berkeley-Fermilab-Princeton-experiment[12] (BFP) and the two experiments at CERN by the European Muon Collaboration (EMC) (Ref. 13) and by the CERN-Dubna-Munich-Saclay Collaboration.[14] The objective of these experiments is not only to measure scaling violations in regular deep-inelastic processes but also to study the multimuon signals with a view to extracting the virtual photoproduction of charmed and/or bottom-flavored particles.[15] The analysis of multimuon events is complicated due to the abundance of possible production processes. One signal which is clean is J/Ψ production and some beautiful results on the reaction $\mu N \to \mu(J/\Psi)X$ have already appeared.[16] The CERN experiments[13,14] mentioned above have rather complicated cuts due to the geometrical acceptance of their detectors. This means that all muons are not positively identified and some leakage, say from trimuons into dimuons, becomes possible. Hence it is crucial to understand the effect of cuts on the experimental signals.

The actual calculation of the Bethe-Heitler-type diagrams involved in Fig. 1 is not complicated. We have already made similar calculations[17] for e^+e^- colliding-beam two-photon processes and can readily adapt those programs. The only real complication is caused by the severe peaking of the integration variables due to the extremely small momentum transfers involved. Such complications have been recognized many times before.[18] We mention in particular the work of Chen *et al.*,[19] who calculated the cross sections for the reactions $pp \to \mu^+\mu^- pp$, $pp \to \mu^+\mu^- pX$, and $pp \to \mu^+\mu^- X$ at high energies. They carried out some integrations analytically so

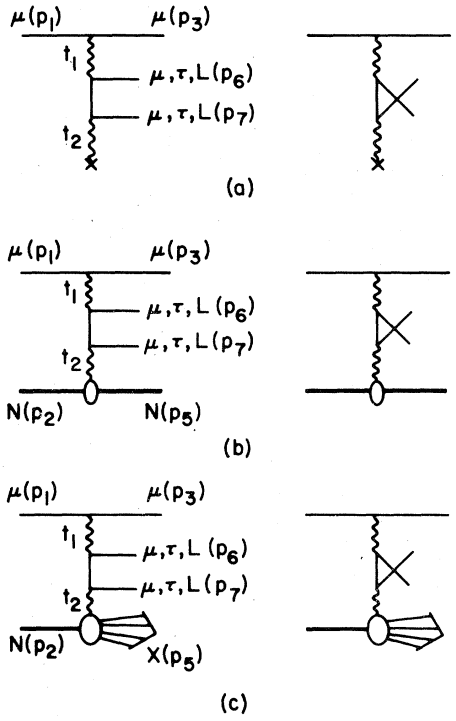

FIG. 1. The Bethe-Heitler diagrams for an incident muon on (a) a nucleus, (b) a nucleon (elastic), and (c) a nucleon (deep inelastic).

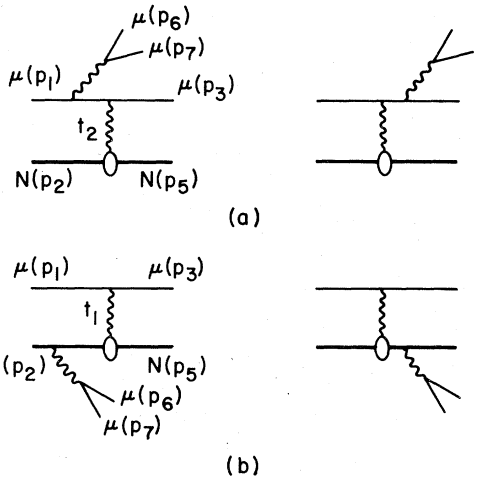

FIG. 2. The charge-conjugation-odd diagrams involving radiation of muon pairs from (a) the initial and final muons, and (b) the initial and final hadrons.

that they could get extremely good accuracy for the distribution in the mass of the dimuon pair. We have been able to use their cross section and our previous e^+e^- cross sections to thoroughly check our computer programs.

For completeness we also give some cross sections for the C-odd production of muon pairs. These arise from the muon radiation diagrams in Fig. 2(a) and the Compton radiation diagrams in Fig. 2(b). The muon radiation diagrams are exactly calculable as the photon-hadron vertex is completely known. The Compton radiation graphs can only be treated in a model-dependent fashion (see Ref. 6). These C-odd diagrams give much smaller cross sections than the C-even diagrams because the muon and/or quark propagators are pushed far off mass shell. Therefore, for heavy-lepton production we will simply drop these diagrams and concentrate on the C-even production mechanism.

We present results for dilepton production via coherent Coulomb scattering, incoherent proton and neutron scattering, and deep-inelastic scattering. Given that quantum electrodynamics adequately describes leptonic interactions in the energy range under consideration, the only ambiguity arises from the proton structure functions. We have used the latest available data on scaling violations[20] and the value of $R = \sigma_L/\sigma_T$.[21] For the reaction involving $\tau^+\tau^-$ and L^+L^- pairs we also add their leptonic decays. This work therefore complements our previous work on the real photoproduction of $\tau^+\tau^-$ pairs.[22] It may be possible for the experimental groups to identify events with leptonic decays, using the fact that four neutrinos are emitted, so a large fraction of the beam energy is not detected.

To summarize, therefore, we concentrate on those cross sections which are purely electromagnetic and therefore calculable. The decay matrix element and branching ratio for τ leptons are known[23] so the leptonic spectra can be given without any ambiguity. We suppose that the heavier leptons decay in the same fashion. We chose the mass 4.8 GeV/c^2 for the heavy lepton just to give a mass around that of the b quark. We are not claiming that such a particle exists but we simply use this mass to study the kinematical effects of heavy-mass-lepton production. It is unlikely that even heavier-mass-lepton pairs can be detected by Bethe-Heitler processes because the cross section drops off too quickly. However, it is interesting to give some results with future facilities in mind, i.e., the 1-TeV proton beam at Fermilab and possible ep colliding-ring machines.

Heavy-quark production is a quantum-chromodynamics (QCD) problem and is not discussed. The photon-gluon model is similar in spirit to the QED Bethe-Heitler reaction and the distributions tend to be similar. In Sec. II we give some details of the various structure functions

which are used and then give the results in Secs. III and IV.

II. CALCULATIONAL DETAILS

The calculation of the square of the Feynman diagrams in Fig. 1 is most easily done with the help of the SCHOONSCHIP trace program written by Veltman.[24] In a previous paper we computed the square of all the C-even diagrams in Fig. 1 *and* the C-odd diagrams in Fig. 2 for e^+e^- collisions.[17] Of course, the interference terms vanish in the total cross section but do contribute if the detector is charge asymmetric. To repeat this calculation for μp collisions with unequal masses would just give a rather long trace which can then be integrated to give the cross sections. We decided to try another method of calculation to see if we could reduce computing time and also learn some new techniques.

Several years ago, before the advent of the algebraic trace programs, it was suggested that calculations involving many Feynman diagrams could be simplified by employing representations for the spinors and evaluating the amplitudes directly by multiplying out the matrices. Then one takes the square of the real and imaginary parts of the final amplitudes to calculate the cross section. Programs were written to do this[1,2,4] and later used to study the effects of Fermi-Dirac statistics in trimuon production.[9] Although such programs are available, we have not found them to be very efficient at high energies. The reason for this is that the integration variables chosen are not the most efficient. In such cases correlations are introduced so it is difficult to achieve accurate results when the beam energies are large. (Remember there have been discussions of ep colliding rings where $s = 10^4$–10^5 GeV^2). This is basically the reason why we had to redo several two-photon physics calculations so that they could be handled at PETRA-PEP energies.[17] Our trick is to use multiperipheral invariants as integration variables and then remap onto the laboratory energies and angles. When such methods are used, the peaking in the cross sections is easily controlled and the rest of the calculation can be done either by evaluating the amplitudes using matrix methods, or the squares of the amplitudes using trace techniques. If matrix methods are used then we get the best of both possible worlds because cancellations occur in the matrix element M rather than in M^2. Also, matrix methods turn out to be just as efficient in terms of computer time and they allow one to trivially give results for polarized beams.

Vermaseren[25] has recently written a useful set of subroutines for the matrix multiplication of vertices and propagators in QED. These routines are now used by the experimental groups at PETRA who are studying two-photon physics processes in e^+e^- colliding beams. We have modified these routines to handle the photon-hadron vertex both with elastic and inelastic form factors. It is then easy to calculate the cross sections for the diagrams depicted in Figs. 1 and 2. The numerical work is done by Monte Carlo methods so that all possible distributions can be extracted. We cross checked our results, using previous results for e^+e^- and pp colliding beams and muon pair radiation by muons.[6] The fact that practically all of the calculations were therefore done by two different methods gives us good confidence that our results are correct and accurate to an error of less than five percent. Although we only present results here for the region of energy below 600 GeV, our program can handle much higher beam energies.

We start with the pointlike proton. In this case no form factors are employed and the resulting cross section is a good benchmark for all the other cases. Then we proceed to give results for proton and neutron targets, using the standard dipole form factors ($t = q^2 < 0$)

$$G_{E,p} = \frac{G_{M,p}}{2.79} = -\frac{G_{M,n}}{1.91} = \left(1 - \frac{t}{0.71\ \text{GeV}^2}\right)^{-2}, \qquad (2.1)$$

$$G_{E,n} = 0.$$

These will be referred to as the incoherent proton and neutron form factors. The resulting incoherent cross sections are given per proton or per neutron.

Next we turn to the coherent scattering from a nuclear target. For this case we use the exponential form factor

$$F(\vec{q}^2) = \exp(-\tfrac{1}{6}a^2 |\vec{q}|^2) \qquad (2.2)$$

with

$$a = (\tfrac{3}{5})^{1/2}(1.3A^{1/3}) \times 10^{-13}\ \text{cm},$$

where A is the atomic number. Of course, one should multiply the final result by Z^2 to get the total coherent cross section. This exponential is not a good fit to the real Fermi form factor, which has oscillations caused by the sharp edge of the nuclear charge distribution. When experimental cuts are imposed, the momentum transfer to the nucleus is larger and these secondary oscillations become important. We have studied this effect primarily using an iron target because this is the material used in the muon experiments, and we find that we can easily be wrong by a factor of 2 in the cross section if the secondary peaks

are neglected. For completeness we give a good fit to the Fermi form factor in the three different momentum transfer ranges. Using the notation $T = |\vec{q}|^2 > 0$, then

$$F(T) = \frac{\exp[-\frac{1}{6}(0.58+0.82A^{1/3})^2 T \times 10^{-26}\ \text{cm}^2]}{(1+T\times 10^{45.92T})}$$

for $0 < T < 0.044$ $(\text{GeV}/c)^2$,

$$F(T) = -0.283\ 516 + 11.17128T - 122.791T^2 + 413.824T^3$$

for $0.044 < T < 0.132$ $(\text{GeV}/c)^2$, and

$$F(T) = -0.158\,323 + 2.392\,78T - 11.267\,49T^2 + 16.9721T^3$$

for $0.132 < T < 0.25$ $(\text{GeV}/c)^2$. (2.3)

A plot of the exact $F(T)$ is shown in Fig. 3, where it is compared with the fit given by Eq. (2.2). The fit used by Barger *et al.*,[7] namely, $F(T) = \exp(-\frac{1}{6}b^2T)/(1+\frac{1}{6}c^2T)$ with $c = 1.07A^{1/3}$ fm and $b = 24$ fm is also shown as the dot-dashed line in Fig. 3. This fit falls off much faster than ours and leads to a smaller value for the coherent cross section. Our results are approximately a factor of 3 times larger. The disagreement is worse in a realistic situation where the small-T region would be effectively excluded by cuts on the primary muon energy and/or angle. Our form factor is still finite for larger values of T. Actually it may be possible to use the trimuon coherent cross section to investigate the shape of the Fermi form factor at larger values of T. In an actual experiment of course there will be other contributions at small T due to the inelastic scattering to excited states of the nucleus. Such problems have been touched upon by Tasi[26] for the case of real photoproduction of muon pairs. In practice one needs to average over the contributions of several excited states and add the effects due to Fermi motion and the Pauli principle. It is not yet clear whether such refinements are required for heavy-lepton production so we have not investigated the matter any further. We present total cross sections (per proton) for three different nuclei, namely, alumium ($Z = 13$, $A = 27$), iron ($Z = 26$, $A = 56$), and lead ($Z = 82$, $A = 207$), but only give distributions for iron.

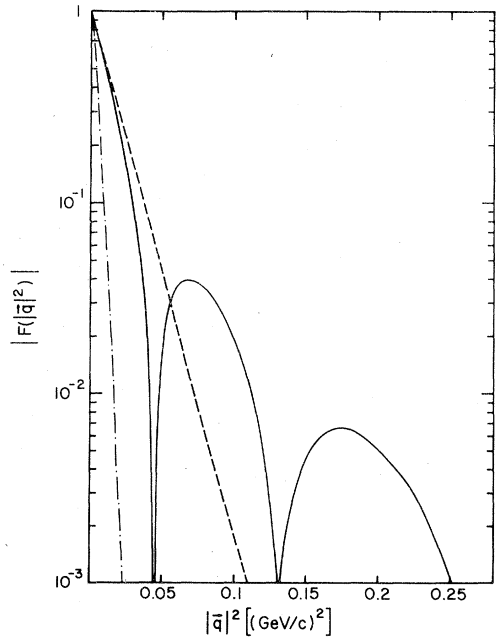

FIG. 3. Fits to the modulus of the Fermi form factor for an iron nucleus. The exact form factor is given by the solid line and the dashed line gives the fit in Eq. (2.2). The fit in Eq. (2.3) also covers the second and third oscillation. The dot-dashed curve shows the fit used by Barger *et al.*

Finally we have to discuss the deep-inelastic scattering cross section for an isoscalar target. For processes involving only a single-photon interaction with the hadron (as in the case of Bethe-Heitler and muon radiative production) the cross section is determined by the deep-inelastic structure functions W_1 and W_2. The phenomenological fits we assume include scaling violations in the form of a Buras-Gaemers parametrization,[27] even though the bulk of the cross section is at relatively low values of $Q^2 = -q^2$. We use a fit to neutrino data involving the variable $\bar{s} = \ln[\ln Q^2/0.47)/\ln(10.64)]$ above $Q^2 = 5$ $(\text{GeV}/c)^2$ and assume exact scaling below $Q^2 = 5$ $(\text{GeV}/c)^2$. The standard factor of 5/18 is then incorporated to change from neutrino to muon scattering. Our parametrization is therefore

$$F_2(x,Q^2) = 3x^{\eta_1(\bar{s})}(1-x)^{\eta_2(\bar{s})}/D(\bar{s}) + A(\bar{s})(1-x)^{B(\bar{s})},$$

where

$$\eta_1(\bar{s}) = 0.56 - 0.147\ \bar{s},$$

$$\eta_2(\bar{s}) = 2.71 + 0.813\ \bar{s},$$

$$D(\bar{s}) = 0.77 + 0.29\ \bar{s},$$

$$A(\bar{s}) = 0.99 + 1.71\ \bar{s},$$

and

$$B(\bar{s}) = 8.1 + 4.76\ \bar{s}.$$

F_1 is given by the usual Callan-Gross relation $2xF_1 = F_2$. In view of the present confusion regarding the value of $R = \sigma_L/\sigma_T$, we decided to choose the canonical value $R = Q^2/\nu^2$ which makes the Callan-Gross relation exact. Once R is bet-

ter known experimentally, this can be incorporated in the calculation. The latest status on R can be found in the review article by Drees.[28] We have compared our $\mu^+\mu^-$ cross-section results with those of Barger *et al.*[7] and find good agreement.

Note that the integration over the invariant mass W is started at the pion threshold $W = M_P + m_\pi$ so that the incoherent and coherent cross sections can be treated independently and added to get the total cross section. Our fit to the structure functions is supposed to average over the contributions of the low-lying resonances.

In Sec. III we present the results of the calculations for an incident muon beam with energy ranging from 50–600 GeV. For completeness we include some results for muon radiative production in scattering on nucleons and nuclear targets. Cross sections for Compton radiation have already been given in Ref. 6.

III. RESULTS FOR CROSS SECTIONS

For clarity we discuss the cross sections for various assumptions about the target in separate subsections. In Figs. 4–7 we present the variation of the total cross sections with energy, for all cases considered, to understand their relative orders of magnitude. The energy variation of the trimuon total cross section is rather weak and reflects a growth as a power of $\ln s$. For this reason we do not expect the distributions to change dramatically once s is sufficiently large that threshold effects can be neglected. In the case of $\tau^+\tau^-$ and L^+L^- cross sections these

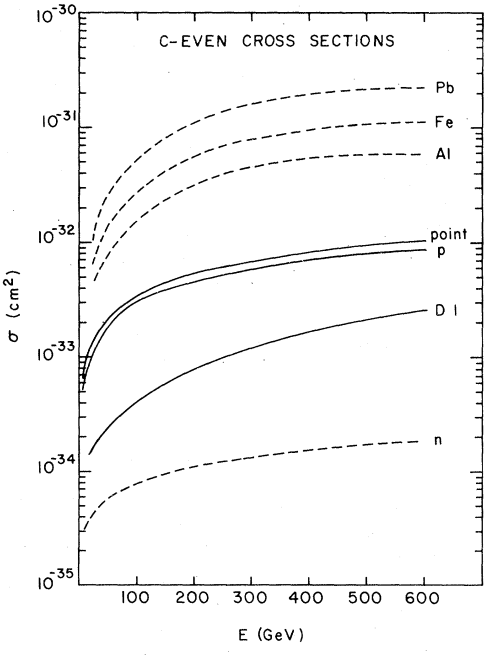

FIG. 4. Total cross sections for the charge-conjugation-even diagrams in Fig. 1. The neutron elastic cross section is denoted by n, the deep-inelastic cross section per nucleon is denoted by DI, the proton cross section is denoted by p, and the coherent cross sections per proton are denoted by their atomic symbols.

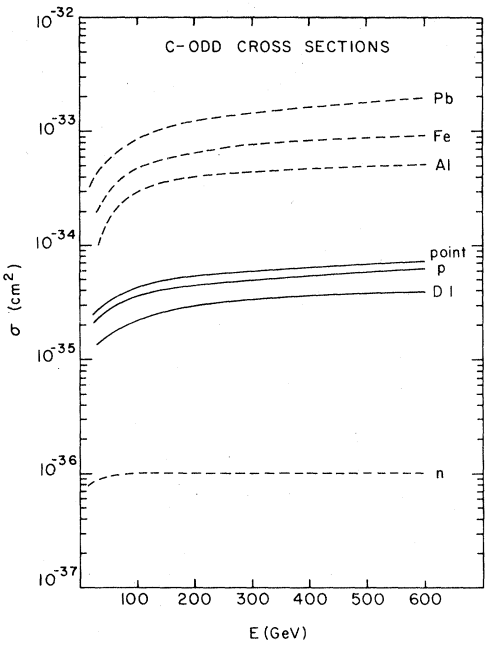

FIG. 5. Total cross sections for the charge-conjugation-odd muon radiation diagrams in Fig. 2. The notation is identical to that in Fig. 4.

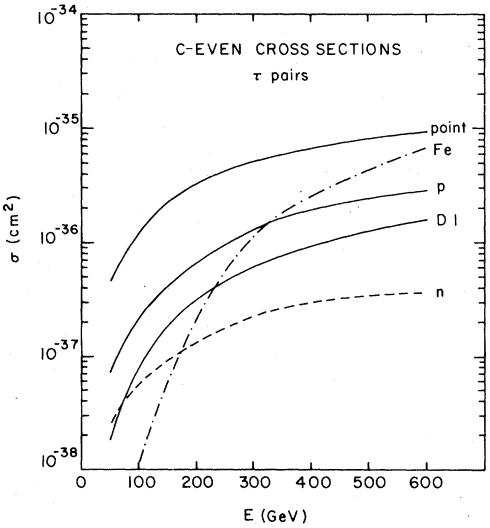

FIG. 6. Total cross sections for the charge-conjugation-even production of $\tau^+\tau^-$ pairs. The notation is identical to that in Fig. 4.

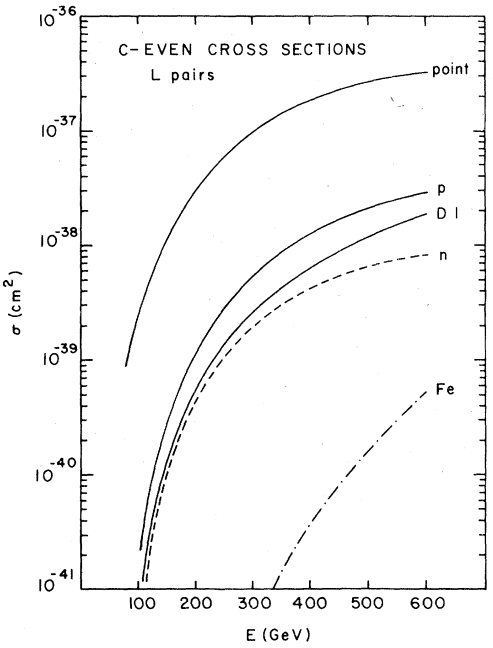

FIG. 7. Total cross sections for the charge-conjugation-even production of L^+L^- pairs. The notation is identical to that in Fig. 4.

threshold effects are very important. The results we give are accurate to approximately five percent.

A. Pointlike cross section

Here we give results for the $\mu^+\mu^-$ total cross sections for the C-even diagrams in Fig. 4 and the C-odd diagrams in Fig. 5. The values obtained give a very good estimate of the basic size of the cross section per proton. Due to the average momentum transfer being so low, we expect the form factors to have only a small effect on this basic cross section. Corresponding results are shown in Fig. 6 for the C-even pointlike production of $\tau^+\tau^-$ pairs and in Fig. 7 for L^+L^- pairs. We take $m_\tau = 1.78\ \mathrm{GeV}/c^2$ and $M_L = 4.8\ \mathrm{GeV}/c^2$. These values are also close to the masses of the charmed and bottom quarks, respectively, so with the minor change of substituting a color factor rather than the square of the electromagnetic charge, these cross sections give approximate QCD predictions for typical gluon-exchange models. To be quantitative, of course, the actual gluon distribution functions must be added, as, for example, in Refs. 7 and 15.

The heavy-lepton cross sections are reduced near threshold by the limitation on the minimum momentum transfer at low energies. However, the QCD color factor gives a large increase, so it turns out that the cross section for, say, D-meson production in the gluon-fusion model is approximately equal to the basic $\mu^+\mu^-$ total cross section.

The C-odd muon radiation diagrams lead to cross sections which are approximately a factor of 100 less than the cross sections for the C-even diagrams. These cross sections are plotted in Fig. 5. The suppression is due to the lepton propagators in Fig. 2(a) being pushed away from their mass shells. This effect gets worse as we change the mass of the radiated pair from $m_{\mu\mu}$ to $m_{\tau\tau}$ or m_{LL}. The latter cross sections are so small that they can be safely neglected from further consideration.

B. Proton and neutron dipole form factors

We first note that the $\mu^+\mu^-$ cross sections per proton are not much lower than the point-proton cross sections. This is because the point cross sections fall off rather severely in q^2 due to the photon propagator and thus only the low-q^2 regions contribute. This also explains why the neutron cross section is so low. The neutron undergoes only magnetic scattering which is dominant only at wide angles or large q^2. We see from the results in Figs. 4–7 that the incoherent cross section for scattering per neutron is generally negligible compared to the incoherent scattering from protons. This conclusion may not be entirely correct in the case that cuts remove the low-q^2 region of phase space. Then the neutron scattering could be more important relative to the proton scattering.

C. Coulomb scattering

The scattering from the Coulomb field of the nucleus produces the largest cross sections for muon tridents. This is only partly due to the additional factor of Z relative to the incoherent proton and neutron results. Note that in Figs. 4–7 we have only added one factor of Z, so that both σ_{coh} and σ_p are given per proton. We see from Figs. 4 and 5 that the total cross sections on Al, Fe, and Pb targets are approximately seven, eleven, and twenty-three times the point cross sections per proton in the asymptotic region. As far as the various form factors are concerned, there is little difference in the total cross section because all fits cover the small-$|\vec{q}|^2$ region rather well. Once higher-$|\vec{q}|^2$ values become important we expect changes due to the approximate nature of the expotential form factor relative to the real behavior of the Fermi form factor. In those regions there can be differences by factors of 2 between the cross sections, depending upon the choice of form factor.

The Coulomb scattering is not the dominant mechanism for producing $\tau^+\tau^-$ and L^+L^- pairs because of t_{min} effects. The severe suppression at low energies can be clearly seen in Figs. 6 and 7. The coherent $\tau^+\tau^-$ production cross section is only appreciable for muon energies above 300 GeV. The coherent L^+L^- production cross sections are small below 1 TeV.

D. Inelastic scattering on an isoscalar target

The total inelastic cross sections per nucleon computed with the structure functions given in Eq. (2.4) are shown also in Figs. 4–7. Most of the cross section is in the region of low-momentum transfer due to the photon propagator. Therefore, if we do not impose a cut to force Q^2 to be large, the inelastic cross sections are small and generally fall somewhere between the proton and neutron results. At very low beam energies they are actually larger than the neutron cross sections, but in that region, all cross sections are too small to be of interest.

The basic cross sections per nucleon for τ-pair production are approximately several picobarns at 500-GeV beam energy. This is a factor of 10^3 smaller than the cross sections for $\mu^+\mu^-$ pairs. The corresponding cross sections for L-pair production are several times 10^{-38} cm^2, which means that they are probably unmeasurable with present muon-beam facilities.

To summarize this section we give the formula for the total cross section arising from the addition of the various contributions. On a nucleus with atomic number A and charge Z the final cross section is

$$\sigma_{TOT} = Z\sigma_{coh} + Z\sigma_p + (A-Z)\sigma_n + A\sigma_{DI}. \quad (3.1)$$

The deep-inelastic cross section, which is multiplied by A, is therefore just as important as the proton cross section for τ-pair production and L-pair production. The coherent nuclear cross section is important for τ-pair production on an Fe target but is negligible for L-pair production.

IV. RESULTS FOR DISTRIBUTIONS

We will now present some results for differential distributions. Barger *et al.*[7] have given results for regular $\mu^+\mu^-$ production at 280-GeV beam energy so we concentrate on the results for heavy leptons and their decay products. The incoherent and inelastic cross sections only vary slowly above an energy of, say, 500 GeV, so we choose this value for the beam energy. At this value the total coherent cross section for τ pairs is approximately twice as large as the total inelastic cross section before any cuts are made. However, the distributions for the decay leptons are remarkably similar, due primarily to the large value of T_{min}. In the case of L-pair production, the total deep-inelastic cross section is much larger than the corresponding coherent cross section. For this reason we only present results for deep-inelastic scattering which allows us to reduce the number of plots. Any experimental group which requires more detailed information can receive a copy of the computer program upon request.

The decay modes considered are $\tau^+ \to \bar{\nu}_\tau \mu^+ \nu_\mu$, $\tau^- \to \nu_\tau \mu^- \bar{\nu}_\mu$ with corresponding decays for the L leptons. We assume that the final daughter muons are detected together with the fast scattered muon at the primary vertex. The addition of the $V-A$ decays is standard, so we do not need to discuss it. The normalization is done with respect to the total decay rate, so there are two additional factors of the branching ratio into the muonic channel. We normalize the differential distributions to the production cross section so that we can easily compare the shapes of the plots.

In Fig. 8 we show the distribution of the fast scattered muon for the reactions leading to $\mu^+\mu^-$, $\tau^+\tau^-$, and L^+L^- final states. The trend in the plots is obvious: as we produce heavier leptons, the energy available for the primary muon falls severely. In the same figure we also give the visible-energy distribution. For muons this is a δ function at 500 GeV. The other processes lead to four invisible neutrinos, which carry away a significant fraction of the beam energy, so E_{vis} does not add up to 500 GeV.

In Figs. 9(a) and 9(b) we compare the energies of the produced parent μ, τ, or L with those of

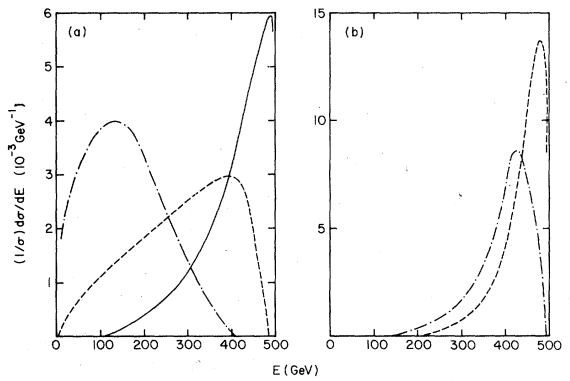

FIG. 8. (a) The distributions in energy of the scattered fast muon in the reactions $\mu p \to \mu\mu^+\mu^- X$ (solid line), $\mu p \to \mu\tau^+\tau^- X$ (dashed line), and $\mu p \to \mu L^+ L^- X$ (dot-dashed line). The beam energy is 500 GeV. (b) The distributions in the total visible energy of the detected hadrons and muons from the τ-decay reaction (dashed line) and the L-decay reaction (dot-dashed line).

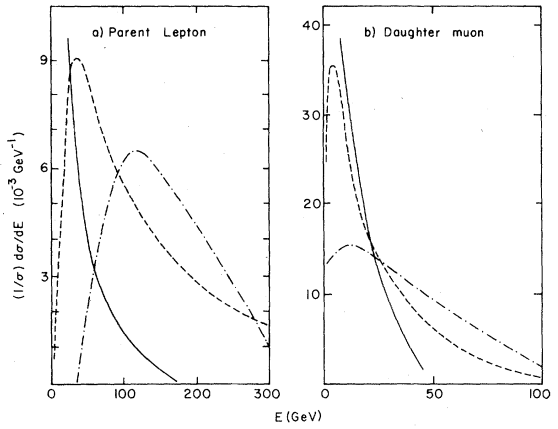

FIG. 9. (a) The energy distribution of the parent slow leptons. (b) The energy distribution of the daughter leptons. The notation is the same as in Fig. 8.

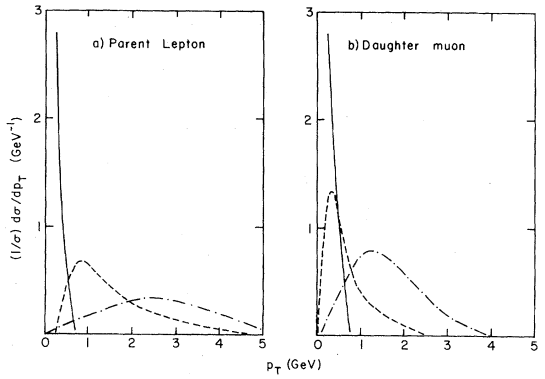

FIG. 11. The transverse-momentum distributions with respect to the beam direction of (a) the parent leptons, and (b) the decay leptons. The notation is the same as in Fig. 8.

the daughters. Note that the scale changes in going from (a) to (b) and we show the scattered muon energy in both plots. Obviously the primary lepton carries more energy as its mass is increased, but because it then shares the energy among three daughter particles, the secondary-muon energy peaks at smaller values.

From a study of the invariant masses we found that the 3μ, $\mu\tau^+\tau^-$, and μL^+L^- invariant masses were not significantly different from the masses of the $\mu^+\mu^-$, $\tau^+\tau^-$, and L^+L^- pairs. Therefore, we only give the distributions for the latter. The curves for the parents can be seen in Fig. 10(a) while the daughter distributions are given in Fig. 10(b). Note that the thresholds in Fig. 10(a) are caused by the particle masses and they disappear in Fig. 10(b).

The transverse-momentum distributions, which we now show in Figs. 11(a) and 11(b), basically reflect the large masses involved in the reaction. The $p_\perp$ distributions are given with respect to the beam axis and have tails stretching out to several GeV/c. It is debatable whether the daughter $p_\perp$ distributions can distinguish between heavy-lepton production and charm production at the hadronic vertex. A cut on $E_{\rm vis}$ would be helpful to separate these two signals because the $c\bar{c}$ events tend to be very inelastic and lose energy into two neutrinos while the $\tau^+\tau^-$ events have four missing neutrinos.

For completeness we have examined other distributions to see if there is any characteristic feature which can be exploited. The azimuthal-angle distribution between the $p_\perp$ of the leading scattered muon and the sum of the other two $p_\perp$ vectors may turn out to be useful. These distributions are given in Fig. 12(a) for the parent

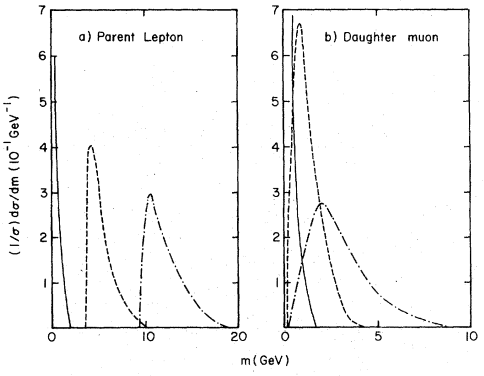

FIG. 10. (a) The mass distributions for the produced parent leptons, and (b) the mass distributions for the daughter muons. The notation is the same as in Fig. 8.

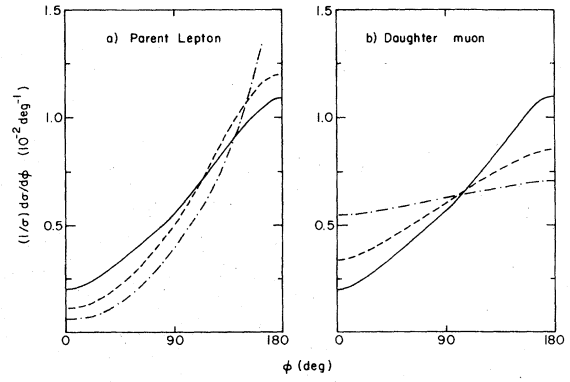

FIG. 12. The distributions in the azimuthal angle $\phi = \phi_{1,(2+3)}$ between the $p_\perp$ vector for the fast primary muon and $p_\perp$ vector for the secondary pair. The parent distribution is shown in (a), and the daughter distribution in (b). The notation is the same as in Fig. 8.

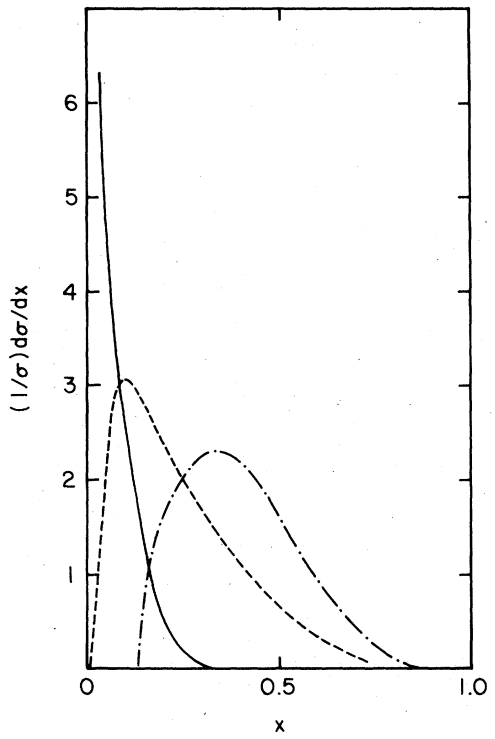

FIG. 13. The $x = Q^2/2M\nu$ distributions for the three reactions. The notation is the same as in Fig. 8.

particles and in Fig. 12(b) for the daughters. The sharp peaking in Fig. 12(a) is caused by the $p_\perp$ balance between the two leptons and the scattered muon. This peaking is substantially reduced when we look at the daughter distributions. The corresponding ϕ plots for $c\bar{c}$ production probably reflect similar features because the basic production mechanism seems to be of a diffractive, low-x behavior. The ϕ distributions were very useful in distinguishing between different trimuon production mechanisms in neutrino physics.[29]

Finally, for completeness, we plot the *theoretical* $x = Q^2/2M\nu$ distribution for the reaction in Fig. 13. Q^2 and ν refer to the momentum transfer and energy transfer at the photon-hadron vertex. The normal $\mu^+\mu^-$ pair cross section peaks sharply at small x. As we produce heavier masses the effective Q^2 is larger so the important region moves out to a larger x. The reason we stress that this distribution is only theoretical is that there will be missing energy when heavy leptons are produced so the actual plot will involve a visible x rather than a real x. Also, the experimenters will probably define x with respect to the leading muon and that is a different variable entirely.

The distributions we have presented above may be useful in trying to extract a heavy-lepton signal in μp reactions. However, the largest cross section in this field is for heavy-quark production because the QCD coupling constant is larger than the QED.[15] In the event that some peculiar trimuon events are seen with large energy loss, then there is a good probability that heavy-lepton production and decay is responsible.

ACKNOWLEDGMENTS

We would like to acknowledge discussions on muon reactions with K. Johnson, T. Sloan, and J. Vermaseren. This research is supported in part by the National Science Foundation under Grant No. PHY-79-06376.

[1]S. Brodsky and S. Ting, Phys. Rev. 145, 1018 (1966).
[2]J. D. Bjorken and M. Chen, Phys. Rev. 154, 1335 (1967).
[3]G. R. Henry, Phys. Rev. 154, 1534 (1967).
[4]M. Tannenbaum, Phys. Rev. 167, 1308 (1968).
[5]S. Homma, A. Itano, K. Nishikawa, and M. Hayashi, Proc. Phys. Soc. Japan 36, 1230 (1974).
[6]V. Ganapathi and J. Smith, Phys. Rev. D 19, 801 (1979); 20, 2213 (1979).
[7]V. Barger, W. Y. Keung, and R. J. N. Phillips, Phys. Rev. D 20, 630 (1979).
[8]C. H. Albright and R. E. Shrock, Phys. Rev. D 19, 2575 (1979).
[9]J. Russell *et al.*, Phys. Rev. Lett. 26, 46 (1971).
[10]J. Le Britton *et al.*, Phys. Rev. D. 23, 1 (1981).
[11]W. Chen and A. van Ginneken, Phys. Rev. Lett. 40, 1417 (1978); D. Bauer *et al.*, *ibid.* 43, 1551 (1979).
[12]M. Strovink *et al.*, in *Proceedings of the 1979 International Symposium on Lepton and Photon Interactions at High Energies, Fermilab*, edited by T. B. W. Kirk and H. D. I. Abarbanel (Fermilab, Batavia, Illinois, 1980), p. 135.
[13]H. E. Stier, in *Proceedings of the 1979 International Symposium on Lepton and Photon Interactions at High Energies, Fermilab* (Ref. 12), p. 123. See also J. J. Aubert *et al.*, Phys. Lett. 94B, 96 (1980); 94B, 101 (1980).
[14]A. C. Benvenuti *et al.*, in *Proceedings of the 1979 International Symposium on Lepton and Photon Interactions at High Energies, Fermilab* (Ref. 12), p. 161.
[15]A photon-gluon-fusion production model for heavy-quark leptoproduction has been discussed by J. P. Leveille and T. Weiler, Nucl. Phys. B147, 147 (1979). The recent results of A. R. Clark *et al.* [Phys. Rev. Lett. 45, 682 (1980)] support this model of charm production.
[16]A. R. Clark *et al.*, Phys. Rev. Lett. 43, 187 (1979); J. J. Aubert *et al.*, Phys. Lett. 89B, 267 (1980).

[17]R. Bhattacharya, J. Smith, and G. Grammer, Phys. Rev. D 15, 3267 (1977); J. Smith, J. A. M. Vermaseren, and G. Grammer, *ibid.* 15, 3280 (1977).
[18]Neutrino dissociation in a Coulomb field is a typical example, see R. W. Brown, R. H. Hobbs, J. Smith, and N. Stanko, Phys. Rev. D 6, 3273 (1972).
[19]M. S. Chen, I. J. Muzinich, H. Terazawa, and T. P. Cheng, Phys. Rev. D 7, 3485 (1973).
[20]J. G. H. de Groot *et al.*, Z. Phys. 1, 143 (1979).
[21]B. A. Gordon *et al.*, Phys. Rev. D 20, 2645 (1979).
[22]J. Smith, A. Soni, and J. A. M. Vermaseren, Phys. Rev. D 15, 648 (1977); Y. Tsai, Report No. SLAC-PUB 2356, 1979 (unpublished).
[23]M. L. Perl *et al.*, Phys. Rev. Lett. 35, 1489 (1976); G. Feldman *et al.*, *ibid.* 38, 117 (1977); M. L. Perl *et al.*, Phys. Lett. 63B, 466 (1976); 70B, 487 (1977); R. Brandelik *et al.*, *ibid.* 73B, 109 (1978).
[24]H. Strubbe, Comput. Phys. Commun. 8, 1 (1974).
[25]J. A. M. Vermaseren (unpublished).
[26]Y. S. Tsai, Rev. Mod. Phys. 46, 815 (1974); 49, 421 (1977).
[27]A. Buras and B. G. F. Gaemers, Nucl. Phys. B132, 249 (1978).
[28]J. Drees, in *Neutrino '79,* proceedings of the International Conference on Neutrinos, Weak Interactions, and Cosmology, Bergen, Norway, 1979, edited by A. Haatuft and C. Jarlskog (Univ. of Bergen, Bergen, 1980), p. 90.
[29]T. Hansl *et al.*, Nucl. Phys. B142, 381 (1978); A. Benvenuti *et al.*, Phys. Rev. Lett. 42, 1024 (1979); G. L. Kane, J. Smith, and J. A. M. Vermaseren, Phys. Rev. D 19, 1978 (1979).